 doi:10.20944/preprints202102.0601.v1

Optical filters with coupled Sagnac loop waveguide reflectors

Hamed Arianfard, Jiayang Wu, and David J. Moss*

Optical Sciences Centre, Swinburne University of Technology, Hawthorn, VIC 3122, Australia.

ABSTRACT

We present theoretical designs of high performance optical filters in integrated silicon photonic nanowire resonators. We use mode interference in formed by zig-zag waveguide coupled Sagnac loop reflectors (ZWC-SLRs), tailored to achieve diverse filtering functions with good performance. These include compact bandpass filters with improved roll-off, optical analogues of Fano resonances with ultrahigh spectral extinction ratios (ERs) and slope rates, and resonance mode splitting with high ERs and low free spectral ranges. The analysis verifies the feasibility of multi-functional integrated photonic filters based on ZWC-SLR resonators for flexible spectral engineering in diverse applications.

Keywords: Integrated optics, resonators, Fano resonance, mode splitting, classical filters.

1. INTRODUCTION

Micro/Nano-scale integrated photonic resonators enable a wide variety of optical functions in photonic integrated circuits [1-6]. Optical bandpass filters (BPFs) are core components in wavelength division multiplexing (WDM) optical communication systems [7]. To date, a variety of approaches to photonic resonators have been pursued in order to increase the optical filter roll-off as well as to achieve a pseudo flat top spectral response. Both of these features are highly attractive for WDM based optical communications systems [8, 9]. However, most approaches to filter design achieve these desired features by cascading many filters in series. This results in a much larger device footprint and is also challenging to realise these features given typical variations in wavelength drift of the different sub-components due to thermal shifting [10].

Fano resonances are fundamental physical phenomena exhibiting a distinctly asymmetric resonant lineshape profile arose from the constructive and destructive interference of a narrow discrete resonance with a broad spectral line or continuum [11-13]. Optical analogues of Fano resonances have been hot research topics in recent years and have found many applications[11, 14].

At the same time, resonance mode splitting is also a fundamental phenomenon in photonic resonators that occurs when two or more mutually coupled modes co-exist in the same resonant cavity [15, 16]. Recently, many applications based on mode-split resonators have been introduced due to their capability of providing a reduced free spectral range (FSR) and an increased quality (Q) factor while maintaining a small physical cavity length [17-19]. This yields a compact device footprint, low power consumption, and versatile filter shapes for dense WDM (DWDM) and microwave photonics applications [20, 21].

We reported integrated photonic filters recently [22], that achieved multi-functional performance, using an approach based on cascaded Sagnac loop reflectors (SLRs). These were realized through the use of self-coupled silicon-on-insulator (SOI) nanowires. In this paper, we present a theoretical design and optimization of high performance optical filters using a zig-zag waveguide structure based on coupled Sagnac loop reflectors (ZWC-SLR) [23, 24]. Our approach yields a significant improvement in performance as well as the ability to achieve a wide range filter shapes and functions. The ZWC-SLR resonators are essentially composite filters that consist of a combination of both infinite-impulse-response (IIR) as well as finite-impulse-response (FIR) filter elements, realized both in travelling-wave (TW) as well as standing-wave (SW) filter elements. Our approach yields a much more versatile form of mode interference that results in a significantly enhanced flexibility for a wide range of spectral functions [25-30]. Furthermore, the ability to combine this approach with integrated highly nonlinear thin films [30-39] would offer exciting possibilities for advanced nonlinear integrated devices.

Preprints (www.preprints.org) | NOT PEER-REVIEWED | Posted: 26 February 2021 doi:10.20944/preprints202102.0601.v1

2. DEVICE CONFIGURATION

The schematic configurations of two and three ZWC-SLR resonators are illustrated in Figs. 1(a) and (b), respectively. To model the ZWC-SLR resonators based on the scattering matrix method [22, 23, 25], we use both coupler and waveguide parameters that we list in Table 1. In order to enable us to compare the two more easily, we consider the case where both the two and three SLRs are the same in each of the ZWC-SLR resonators. In other words, this equates to L_{SLRi} (i =1-3) = L_{SLR}, t_{si} (i=1-3) = t_s, and t_{bi} (i=1-3) = t_b.

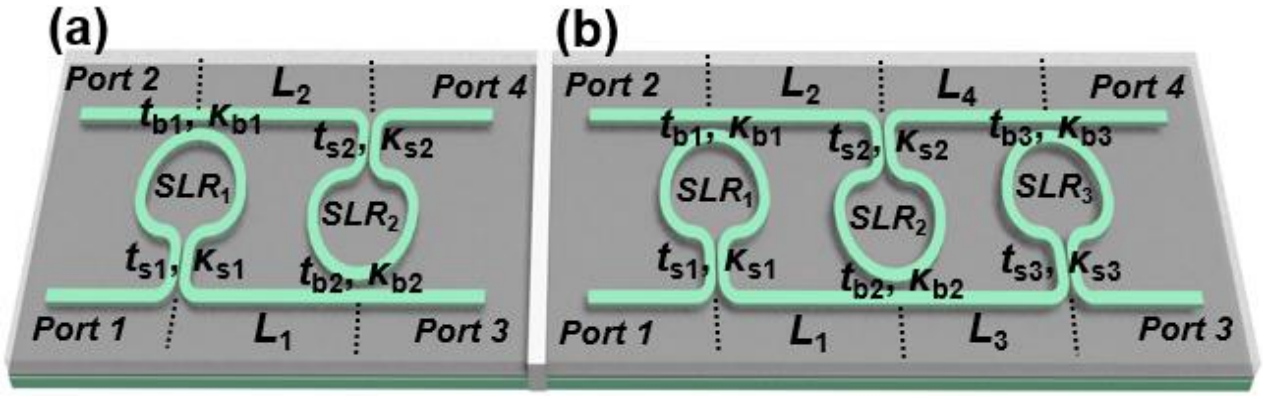

Figure 1. Schematic configuration of (a) two and (b) three ZWC-SLR resonators, respectively. The definitions of t_{si} (i = 1, 2, 3), t_{bi} (i = 1, 2, 3), L_{SLRi} (i = 1, 2, 3), and L_i (i = 1, 2, 3, 4) are given in Table 1.

In the following sections, we tailor the mode interference that occurs in the ZWC-SLR resonators in order to achieve highly performing filters. These including both small footprint BPFs (Section 3), Fano resonances in the optical domain (Section 4), and \ mode splitting of the resonances (Section 5). Here, we take values for the design parameters from our previous paper that reported fabricated SOI devices [22, 26]. This includes the propagation loss (α = 55 m^{-1}, i.e., 2.4 dB/cm) and the waveguide group index (n_g = 4.3350, transverse electric (TE) mode). We note that although we focus on the SOI platform here, our approach is universal and applicable to any integrated platform that can achieve similar performance as SOI.

Table 1. Definitions of structural parameters of the ZWC-SLR resonators

Waveguides	**Length**	**Transmission factor** [a]	**Phase shift** [b]
Bus waveguides between SLRs (i = 1, 2, 3, 4)	L_i	a_i	φ_i
Sagnac loop in SLR_i (i = 1, 2, 3)	L_{SLRi}	a_{si}	φ_{si}
Directional couplers	Field transmission coefficient [c]	Field cross-coupling coefficient [c]	
Coupler in SLR_i (i = 1, 2, 3)	t_{si}	k_{si}	
Coupler between SLR_i and bus waveguide (i = 1, 2, 3)	t_{bi}	k_{bi}	

[a] a_i = exp (-αL_i / 2), a_{si} = exp (-αL_{SLRi} / 2), α is the power propagation loss factor.

[b] $\varphi_i = 2\pi n_g L_i / \lambda$, $\varphi_{si} = 2\pi n_g L_{SLRi} / \lambda$, n_g is the group index and λ is the wavelength.

[c] $t_{si}^2 + \kappa_{si}^2 = 1$ and $t_{bi}^2 + \kappa_{bi}^2 = 1$ for lossless coupling are assumed for all the directional couplers.

3. COMPACT BANDPASS FILTERS WITH IMPROVED ROLL-OFF

Here, the mode interference between two ZWC-SLR resonators are tailored in order to achieve BPFs with enhanced roll-off and a smaller footprint. Figures 2(a) and (b) illustrate the transmission power spectrum as well as the group delay response for both ZWC -SLR resonators, measured from Port 1 to 2, across a range in wavelengths from 1548.9 nm to 1551.2 nm. We achieve very wide as well as flat rejection stopbands together with a passband that features a

Preprints (www.preprints.org) | NOT PEER-REVIEWED | Posted: 26 February 2021 doi:10.20944/preprints202102.0601.v1

significantly enhanced roll-off. These features are a result of coherent mode interference that occurs within both ZWC - SLR resonators. For this case we took the structural parameters to be $L_{SLR} = L = 100$ µm, $t_s = t_b = 0.78$.

To assess the quantitative increase in roll-off of the filters, we compared the BW (3dB) of the BPF that employed two ZWC-SLRs (2-ZWC-SLRs) with BPFs based on different approaches using photonic integrated resonators, such as a single add-drop MRR (1-MRR) [27, 28], as well as dual cascaded SLRs (2-C-SLRs) [29], and 3 cascaded SLRs (3-C-SLRs) [22], and finally dual parallel coupled MRRs (2-MRRs) [27, 28]. To facilitate the comparison, these filters were based on identical SOI nano waveguides with the same parameters including $n_g = 4.3350$ and a loss of $\alpha = 55$ m^{-1}. Figure 3(a) shows the power transmission spectra of the BPFs for the different configurations outlined above. The filter spectra for all of the

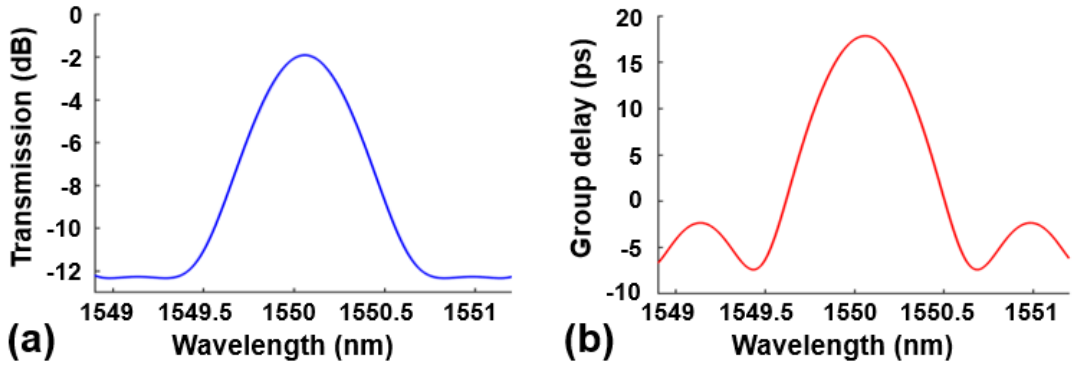

Figure 2. (a) Power transmission spectra of the two ZWC-SLR resonator from Port 1 to Port 2 in the wavelength range of 1548.9 nm –1551.2 nm when $L_{SLR} = L = 100$ µm, $t_s = t_b = 0.78$. (b) Group delay of the BPF in (a).

devices were normalized so that they had the same ER of 10.36 dB as well as the same full width minimum of 230.6 GHz as for the BPF in Fig. 2(a). The associated 3-dB BWs are shown in Fig. 3(b). Clearly, the BPF based on the dual ZWC-SLR resonator achieves the largest 3-dB BW as well as the highest roll-off. This results from the enhanced mode interference that occurs in this compact device that only involves two SLRs.

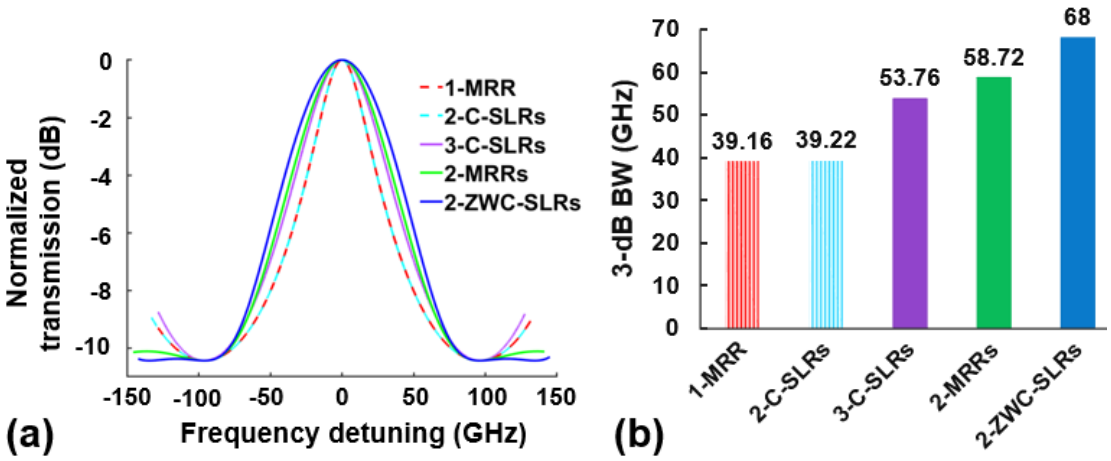

Figure 3. (a) Normalized transmission spectra of BPFs based on various types of integrated photonic resonators, including single add-drop MRR (1-MRR), two cascaded SLRs (2-C-SLRs), three cascaded SLRs (3-C-SLRs), two parallel coupled MRRs (2-MRRs) and two ZWC-SLRs (2-ZWC-SLRs). (b) 3-dB BWs of the BPFs in (a).

4. ULTRA-SHARP FANO RESONANCES

Here, we design the 3 ZWC-SLR resonator spectral response in order to achieve optical versions of Fano resonances that exhibit high ERs as well as high SRs. The transmission power spectrum between Port 2 and 4 of the 3 ZWC-SLR resonator is shown in Fig. 4(a). Clearly there are periodic Fano resonances with asymmetric identical resonant line-shapes within each period. The device structural parameters are $L_{SLR} = L_{1,2,3,4} = 115$ µm, $t_s = 0.743$, and $t_b = 0.994$. The

Preprints (www.preprints.org) | NOT PEER-REVIEWED | Posted: 26 February 2021 doi:10.20944/preprints202102.0601.v1

FSR is about 200 GHz, which equals the sum of the two wavelength spacings (WS1 and WS2). The two WSs are very close to each other (WS1 = 101.71 GHz and WS2 = 98.88 GHz), reflecting the high SR of the Fano resonances.

Figure 4(b) shows a close-up version of Fig. 3(a) for a range of wavelengths of 1549.8 to 1550.65 nm, which shows a Fano resonance with an ultra-high ER of 76.32 dB and an ultra-high SR of 997.66 dB/nm. The ER is defined as the difference between the maximum and the minimum transmission, and the SR is defined to be the ratio between the ER to the difference in wavelength between the peak resonance and the filter notch (i.e., Δλ in Fig. 4(b)). The high ER and SR reflect the high performance of the Fano resonances that arise from a strong interference between the coherent optical mode in the compact resonator with only three SLRs. Further, the periodical filter shape of the zig-zag 3WC-SLR resonator is also useful for applications in WDM systems.

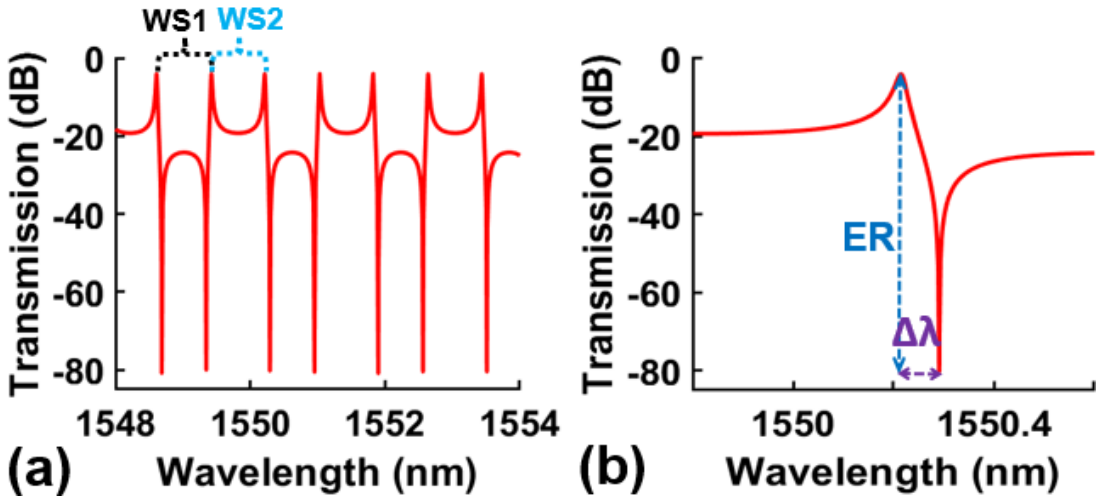

Figure. 4. (a) Power transmission spectrum of the three ZWC-SLR resonator from Port 2 to Port 4 when $L_{SLR} = L_{1,2,3,4}$ = 115 μm, t_s = 0.743, and t_b = 0.994. (b) Zoom-in view of (a) in the wavelength range of 1549.8 nm –1550.65 nm. WS: wavelength spacing. ER: extinction ratio. Δλ: wavelength difference between the resonance peak and notch.

Figure 5(a) compares the power transmission spectra for various t_s (reflectivity of SLRs). we changed only t_s, keeping the other structural parameter the same as those in Fig. 4. The corresponding IL and SR are depicted in Fig. 5(b). The IL increases with t_s, while the SR first increases and then decreases with t_s, achieving a maximum value of 997.66 dB/nm at t_s = 0.743. The non-monotonic relationship between the SR and t_s is a combined result of both a decrease in Δλ and a non-monotonic variation in ER. The latter mainly arises from the difference between the internal (transmission) and external (coupling) cavity loss, which is similar to that for different coupling regimes in microring resonators (MRRs) [30].

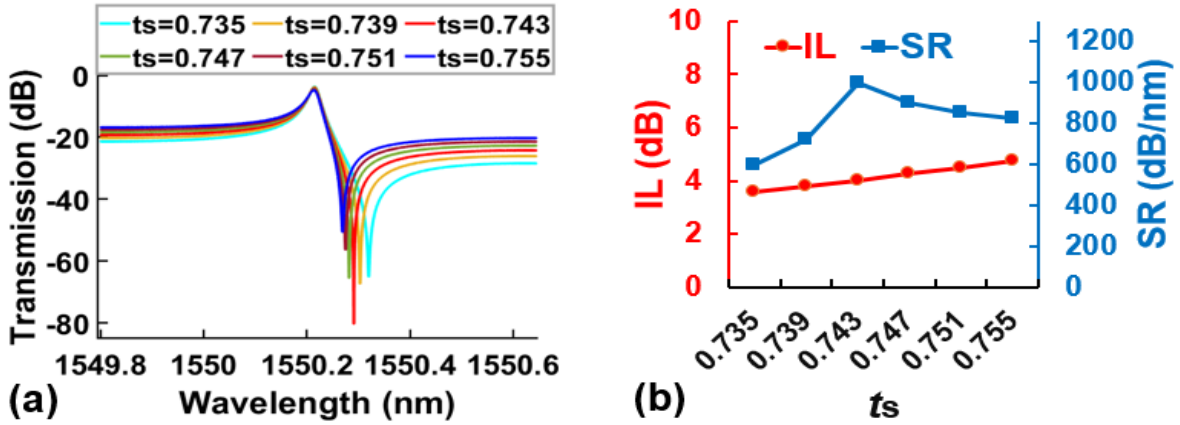

Figure. 5. (a) Power transmission spectra and (b) the corresponding IL and SR for various t_s when t_b = 0.994 and $L_{SLR} = L_{1,2,3,4}$ = 115 μm, respectively.

Preprints (www.preprints.org) | NOT PEER-REVIEWED | Posted: 26 February 2021 doi:10.20944/preprints202102.0601.v1

5. RESONANCE MODE SPLITTING

Here, we adjust the degree of mode interference within the 3 ZWC-SLR resonator in order to realise resonance mode splitting that features both a high ER as well as small FSRs. The resonance mode splitting with multiple densely spaced resonances can break the dependence between the Q factor, FSR, and physical cavity length, thus allowing low FSRs and high Q factors in resonators with a compact footprint. Figure 6(a) shows the transmission power spectrum between Port 2 and Port 4 of the 3 ZWC-SLR resonator. For these calculations we assume values for the device parameters of L_{SLR} = $L_{1,2,3,4}$ = 115 µm, t_s = 0.72, and t_b = 0.99, which were chosen in order to achieve a WS of about 100 GHz between adjacent split resonances. In Fig. 6(a), WS1 = 98.33 GHz and WS2 = 102.26 GHz. There are two split resonances within a FSR of ~ 200.59 GHz. Figure 6(b) shows a close-up view of Fig. 6(a) over a range in wavelengths from 1549 to 1550.7 nm. In Fig. 4(b) for the two split resonances, the IL is 2.02 dB, the Q factor is 6.03 × 10^4, ER1 is 24.65 dB, and ER2 is 27.55 dB.

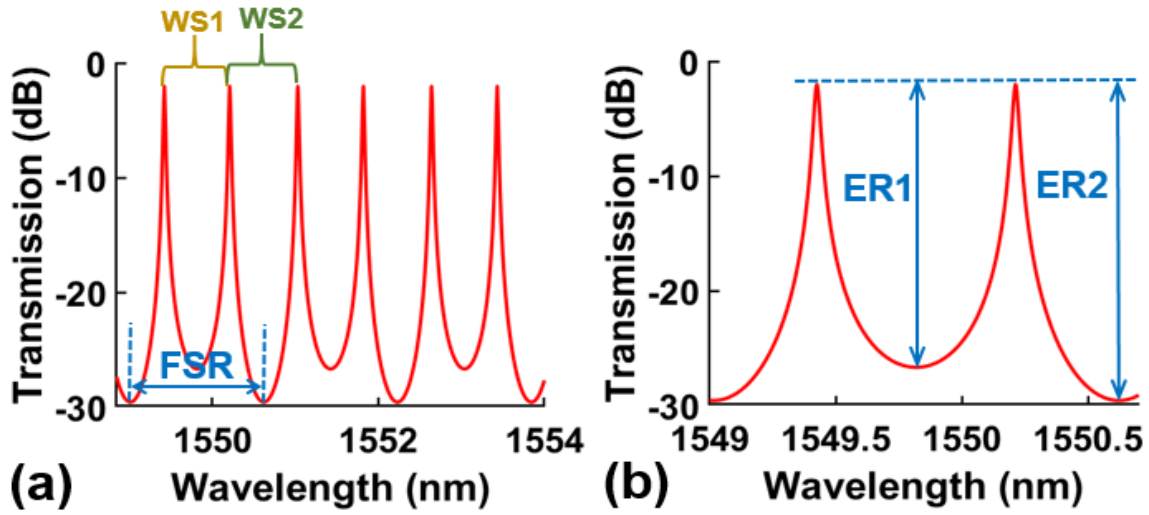

Figure 6. (a) Power transmission spectrum of the three ZWC-SLR resonator from Port 2 to Port 4 when L_{SLR} = $L_{1,2,3,4}$ = 115 µm, t_s = 0.72, and t_b = 0.99. (b) Zoom-in view of (a) in the wavelength range of 1549 nm –1550.7 nm.

Figure 7(a) shows the spectral response for various t_s. we only changed the reflectivity of SLRs, keeping the other structural parameters the same as those in Fig. 6 (a). The Q factor and ERs (ER1 and ER2) as functions of t_s are depicted in Fig. 7(b). As t_s increases, the Q factor slightly decreases while the ER1 and ER2 change more dramatically, resulting in a change in the spectral response towards that of the Fano resonances in Fig. 4(a). The non-monotonic change in ER2 with t_s follows the trend of the SR in Fig. 5(b) for similar reasons. In particular, ER1 equals to ER2 when t_s = 0.7177. Under this condition, the Q factor and effective FSR are ~6.06 × 10^4 and ~100.30 GHz (i.e., half of the FSR in Fig. 6(a)), respectively.

Preprints (www.preprints.org) | NOT PEER-REVIEWED | Posted: 26 February 2021 doi:10.20944/preprints202102.0601.v1

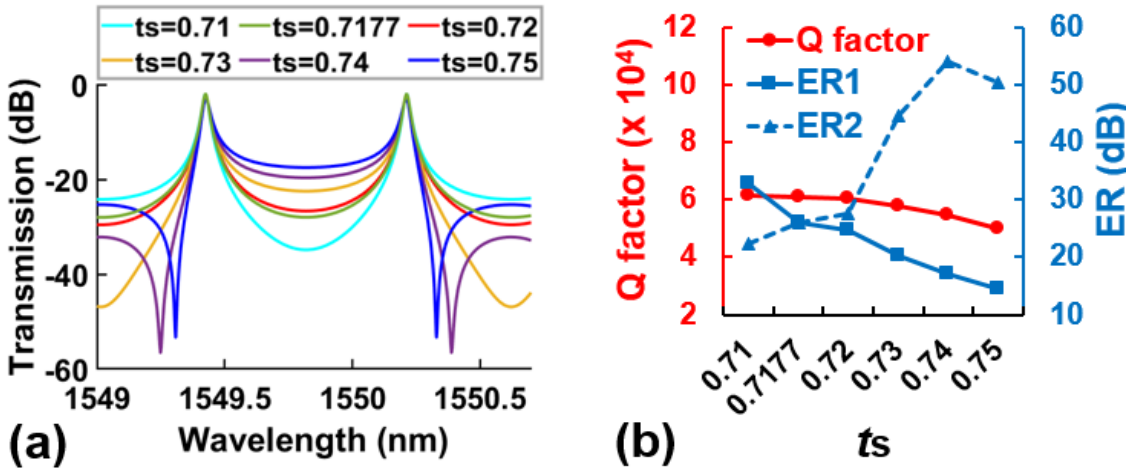

Figure 7. (a) Power transmission spectra of the three ZWC-SLR resonator for various t_s for input from Port 2 to Port 4 when t_b = 0.99 and $L_{SLR} = L_{1,2,3,4}$ = 115 µm. (b) Calculated Q factor and ERs (ER1 and ER2) as functions of t_s for the transmission spectra in (a).

To achieve the same FSR, the circumference of a comparable MRR (with the same waveguide geometry and loss) is 690 µm, which is 6 times the length of the SLRs. This highlights the reduced cavity length enabled by the mode splitting in the 3WC-SLR resonator. On the other hand, the Q factor of a comparable MRR with the same FSR and ER is ~6.08 × 10^4 – almost the same as that of the zig-zag 3WC-SLR resonator. This indicates that the reduced cavity length did not come at the expense of a significant decrease in Q factor.

The number of split resonances can be changed by varying the length of the connecting bus waveguides. Figure 8(a) shows the power transmission spectrum from Port 1 to Port 3 of the three ZWC-SLR resonator. Clearly, there are four split resonances in each FSR. The structural parameters are L_{SLR} = 115 µm, $L_{1,3}$ = 115 µm, $L_{2,4}$ = 230 µm, and $t_s = t_b$ = 0.88. The WSs between the split resonances are WS1 = WS3 = 100.46 GHz and WS2 = 90.37 GHz. Figure 8(b) shows a zoom-in view of Fig. 8(a) in the wavelength range of 1548.7 nm – 1550.7 nm.

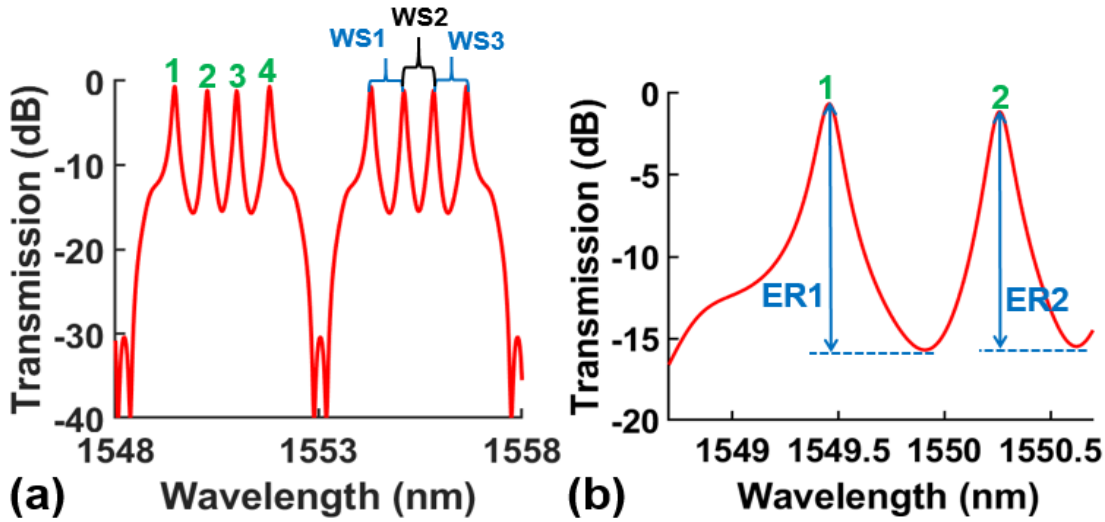

Figure 8. (a) Power transmission spectrum of the three ZWC-SLR resonator from Port 1 to Port 3 when L_{SLR} = 115 µm, $L_{1,3}$ = 115 µm, $L_{2,4}$ = 230 µm, and $t_s = t_b$ = 0.88. (b) Zoom-in view of (a) in the wavelength range of 1548.7 nm –1550.7 nm.

The power transmission spectra for different t_s is shown in Fig. 9(a). The corresponding Q factors (Q1 and Q2) and ERs (ER1 and ER2) for the first two resonances from the left side are shown in Fig. 9(b). In Figs. 9(a) and (b), all the Q factors and ERs decrease with t_s, along with slightly decreased ILs.

Preprints (www.preprints.org) | NOT PEER-REVIEWED | Posted: 26 February 2021 doi:10.20944/preprints202102.0601.v1

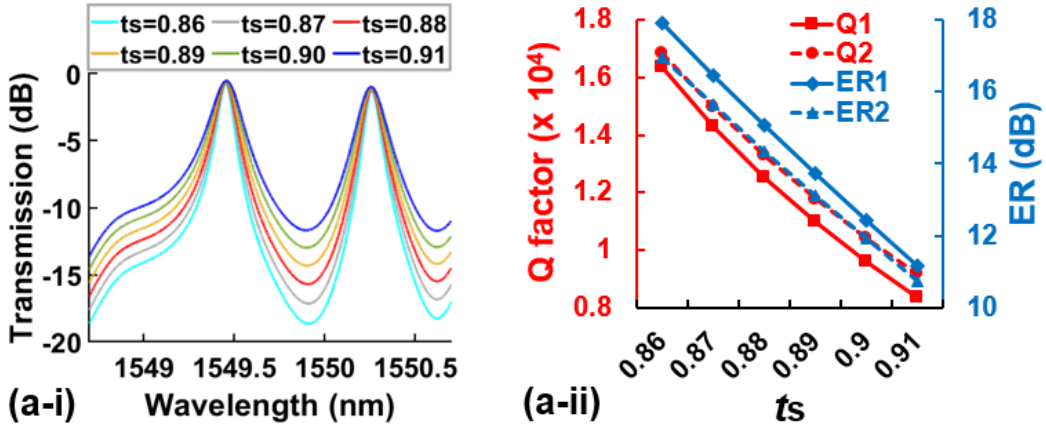

Figure 9. (a) Power transmission spectra of the three ZWC-SLR resonator for various t_s for input from Port 1 to Port 3 when $t_b = 0.88$, $L_{SLR} = 115$ µm, $L_{1,3} = 115$ µm, and $L_{2,4} = 230$ µm. (b) Calculated Q factors (Q1 and Q2) and ERs (ER1 and ER2) as functions of t_s for the transmission spectra in (a).

6. CONCLUSIONS

We perform designs and theoretically study high performance integrated multi-functional photonic filters based on zig-zag cascaded Sagnac Loop Resonators (ZWC-SLRs). We adjust the mode interference within the ZWC-SLR resonators in order to realise different functions for the filters. These include compact bandpass filters with increased roll-off, as well as optical versions of Fano resonances that feature very high ERs and SRs, as well as approaches based on resonant mode splitting with high ERs and low FSRs. Our work shows that ZWC-SLR resonators are very attractive in order to realize robust, adaptable and flexible spectral engineering for a wide range of different applications.

REFRENCES

[1] W. Bogaerts, P. De Heyn, T. Van Vaerenbergh *et al.*, "Silicon microring resonators," Laser & Photonics Reviews, 6(1), 47-73 (2012).

[2] H. Arianfard, B. Khajeheian, and R. Ghayour, "Tunable band (pass and stop) filters based on plasmonic structures using Kerr-type nonlinear rectangular nanocavity," Optical Engineering, 56(12), 121902 (2016).

[3] Z. Yao, K. Wu, B. X. Tan *et al.*, "Integrated silicon photonic microresonators: emerging technologies," IEEE Journal of Selected Topics in Quantum Electronics, 24(6), 1-24 (2018).

[4] J. Wu, Y. Yang, Y. Qu *et al.*, "2D layered graphene oxide films integrated with micro-ring resonators for enhanced nonlinear optics," Small, e1906563 (2020).

[5] H. Arianfard, and R. Ghayour, "Nanoscale plasmonic filter based on coupled metal-insulator-metal waveguides using nonlinear nanoslot resonator," Journal of Nanophotonics, 9(1), 093799 (2014).

[6] J. Wu, P. Cao, X. Hu *et al.*, "Compact tunable silicon photonic differential-equation solver for general linear time-invariant systems," Opt Express, **22**(21), 26254-64 (2014).

[7] C. M. Weinert, [Optical Filters in Wavelength-Division Multiplex Systems] Springer Berlin Heidelberg, Berlin, Heidelberg(2006).

[8] T. Dai, A. Shen, G. Wang *et al.*, "Bandwidth and wavelength tunable optical passband filter based on silicon multiple microring resonators," Optics Letters, 41(20), 4807-4810 (2016).

[9] B. E. Little, S. T. Chu, P. P. Absil *et al.*, "Very high-order microring resonator filters for WDM applications," IEEE Photonics Technology Letters, 16(10), 2263-2265 (2004).

[10] J. Wu, B. Liu, J. Peng *et al.*, "On-Chip tunable second-order differential-equation solver based on a silicon photonic mode-split microresonator," Journal of Lightwave Technology, **33**(17), 3542-3549 (2015).

[11] M. F. Limonov, M. V. Rybin, A. N. Poddubny *et al.*, "Fano resonances in photonics," Nature Photonics, 11, 543 (2017).

[12] J. Chen, F. Gan, Y. Wang *et al.*, "Plasmonic sensing and modulation based on Fano resonances," Advanced Optical Materials, 6(9), 1701152 (2018).

[13] B. Luk'yanchuk, N. I. Zheludev, S. A. Maier *et al.*, "The Fano resonance in plasmonic nanostructures and metamaterials," Nature Materials, 9(9), 707-715 (2010).
[14] E. Kamenetskii, A. Sadreev, and A. Miroshnichenko, [Fano Resonances in Optics and Microwaves: Physics and Applications] Springer International Publishing, (2018).
[15] B. Peng, Ş. K. Özdemir, W. Chen *et al.*, "What is and what is not electromagnetically induced transparency in whispering-gallery microcavities," Nature Communications, 5(1), 5082 (2014).
[16] Q. Li, T. Wang, Y. Su *et al.*, "Coupled mode theory analysis of mode-splitting in coupled cavity system," Optics Express, 18(8), 8367-8382 (2010).
[17] Q. Li, Z. Zhang, F. Liu *et al.*, "Dense wavelength conversion and multicasting in a resonance-split silicon microring," Applied Physics Letters, 93(8), 081113 (2008).
[18] J. Zhu, S. K. Ozdemir, Y.-F. Xiao *et al.*, "On-chip single nanoparticle detection and sizing by mode splitting in an ultrahigh-Q microresonator," Nature Photonics, 4(1), 46-49 (2010).
[19] J. Wu, J. Peng, B. Liu *et al.*, "Passive silicon photonic devices for microwave photonic signal processing," Optics Communications, **373**, 44-52 (2016).
[20] M. C. Souza, G. F. Rezende, L. A. Barea *et al.*, "Spectral engineering with coupled microcavities: active control of resonant mode-splitting," Opt Lett, 40(14), 3332-5 (2015).
[21] L. A. M. Barea, F. Vallini, P. F. Jarschel *et al.*, "Silicon technology compatible photonic molecules for compact optical signal processing," Applied Physics Letters, 103(20), 201102 (2013).
[22] J. Wu, T. Moein, X. Xu *et al.*, "Advanced photonic filters based on cascaded Sagnac loop reflector resonators in silicon-on-insulator nanowires," APL Photonics, **3**(4), 046102 (2018).
[23] H. Arianfard, J. Wu, S. Juodkazis *et al.*, "Advanced multi-functional integrated photonic filters based on coupled Sagnac loop reflectors," Journal of Lightwave Technology, 1-9 (2020). Early access: doi: 10.1109/JLT.2020.3037559.
[24] H. Arianfard, J. Wu, S. Juodkazis, and D.J.Moss, "Three coupled waveguide Sagnac loop reflectors for high performance integrated optical filters," TechRxiv. Preprint. (2020). DOI: 10.36227/techrxiv.13301474.v1.
[25] J. Wu, P. Cao, T. Pan *et al.*, "Compact on-chip 1 × 2 wavelength selective switch based on silicon microring resonator with nested pairs of subrings," Photonics Research, **3**(1), 9-14 (2015).
[26] J. Wu, T. Moein, X. Xu *et al.*, "Micro-ring resonator quality factor enhancement via an integrated Fabry-Perot cavity," APL Photonics, **2**(5), 056103 (2017).
[27] A. Jian, L. Zou, H. Tang *et al.*, "Theoretical analysis of microring resonator-based biosensor with high resolution and free of temperature influence," Optical Engineering, 56(6), 067103 (2017).
[28] M. Borghi, A. Trenti, and L. Pavesi, "Four wave mixing control in a photonic molecule made by silicon microring resonators," Scientific Reports, 9(1), 408 (2019).
[29] X. Sun, L. Zhou, J. Xie *et al.*, "Tunable silicon Fabry-Perot comb filters formed by Sagnac loop mirrors," Optics Letters, 38(4), 567-569 (2013).
[30] J. Wu, P. Cao, X. Hu *et al.*, "Nested configuration of silicon microring resonator with multiple coupling regimes," IEEE Photonics Technology Letters, **25**(6), 580-583 (2013).
[31] Yuning Zhang, Jiayang Wu, Yang Qu, Linnan Jia, Baohua Jia, and David J. Moss, "Design of silicon waveguides integrated with 2D graphene oxide films for Kerr nonlinear optics", TechRxiv. Preprint. (2020). https://doi.org/10.36227/techrxiv.13203278.v1.
[32] Yang Qu, Jiayang Wu, Yuning Zhang, Yao Liang, Baohua Jia, and David J. Moss,"Analysis of four-wave mixing in silicon nitride waveguides integrated with 2D layered graphene oxide films", Journal of Lightwave Technology, Vol. 39, Early Access (2021). DOI: 10.1109/JLT.2021.3059721.
[33] Jiayang Wu, Linnan Jia, Yuning Zhang, Yang Qu, Baohua Jia, and David J. Moss," Graphene oxide: versatile films for flat optics to nonlinear photonic chips", Advanced Materials **32** 2006415, pp.1-29 (2020). DOI:10.1002/adma.202006415.
[34] Y. Qu, J. Wu, Y. Yang, Y. Zhang, Y. Liang, H. El Dirani, R. Crochemore, P. Demongodin, C. Sciancalepore, C. Grillet, C. Monat, B.aohua Jia, and D. J. Moss, "Enhanced nonlinear four-wave mixing in silicon nitride waveguides integrated with 2D layered graphene oxide films", Advanced Optical Materials **8** (21) 2001048 (2020). DOI: 10.1002/adom.202001048.
[35] Linnan Jia, Jiayang Wu, Yunyi Yang, Yi Du, Baohua Jia, David J. Moss, "Large Third-Order Optical Kerr Nonlinearity in Nanometer-Thick $PdSe_2$ 2D Dichalcogenide Films: Implications for Nonlinear Photonic Devices", ACS Applied Nano Materials **3** (7) 6876–6883 June 29 (2020). DOI:10.1021/acsanm.0c01239.

[36] Yuning Zhang, Yang Qu, Jiayang Wu, Linnan Jia, Yunyi Yang, Xingyuan Xu, Baohua Jia, and David J. Moss, "Enhanced Kerr nonlinearity and nonlinear figure of merit in silicon nanowires integrated with 2D graphene oxide films", ACS Applied Materials and Interfaces **12** (29) 33094−33103 June 29 (2020). DOI:10.1021/acsami.0c07852.

[37] Linnan Jia, Dandan Cui, Jiayang Wu, Haifeng Feng, Tieshan Yang, Yunyi Yang, Yi Du, Weichang Hao, Baohua Jia, David J. Moss, "BiOBr nanoflakes with strong nonlinear optical properties towards hybrid integrated photonic devices", Applied Physics Letters Photonics **4** 090802 (2019). DOI: 10.1063/1.5116621

[38] Jiayang Wu, Yunyi Yang, Yang Qu, Xingyuan Xu, Yao Liang, Sai T. Chu, Brent E. Little, Roberto Morandotti, Baohua Jia, and David J. Moss, "Graphene oxide waveguide polarizers and polarization selective micro-ring resonators", Laser and Photonics Reviews **13** (9) 1900056 (2019). DOI:10.1002/lpor.201900056.

[39] Yunyi Yang, Jiayang Wu, Xingyuan Xu, Sai T. Chu, Brent E. Little, Roberto Morandotti, Baohua Jia, and David J. Moss, "Enhanced four-wave mixing in graphene oxide coated waveguides", Applied Physics Letters Photonics **3** 120803 (2018); doi: 10.1063/1.5045509.